Chemical Physics 513 (2018) 246–251

Contents lists available at ScienceDirect

Chemical Physics

journal homepage: www.elsevier.com/locate/chemphys

Chemical potential and free energy of nanoconfined water in Newton black films

S. Di Napoli

Instituto de Nanociencia y Nanotecnología (INN CNEA-CONICET), Buenos Aires, Argentina
Departamento de Física de la Materia Condensada, GIyA-CNEA, Avenida General Paz 1499, (1650) San Martín, Buenos Aires, Argentina

ARTICLE INFO

Keywords:
Newton black films
TIP5P water
Molecular dynamics
Free energy
Chemical potential

ABSTRACT

In this work we investigate possible approximations to the free energy and chemical potential of water within a Newton black film as a natural nanoconfinement. As a first step we explore the different approximations in a sample of 500 water molecules (bulk water), finding that the overlapping distribution method is the more accurate. For the Newton black film we also calculate the free energy profile of the water molecules along the bilayer normal. We obtain that depending on the position of the water molecule inside the bilayer, the excess chemical potential is lower than that of bulk water, suggesting that a water molecule might be more stable inside the Newton black film than in bulk. A charged semiflexible amphiphilic model and the TIP5P model of water are used in our simulations.

1. Introduction

Thin soap films are simple chemical systems which involve the basic physical interactions existing in more complex structures, like, for instance, biological membranes and foams. In foams, the continuous phase forms thin liquid films, which separate the dispersed gaseous bubbles. The stability of foams depends essentially on the stability of these thin films. Black films, the final stages of the thinning of soap films due to the draining of water in the absence of evaporation, are generally formed from solutions of an ionic surfactant in the presence of a salt. Depending on the salt concentration and the temperature, two different types of black films can be observed: common black films (CBF) with thicknesses $D \sim 10$–100 nm and Newton black films (NBF) with thicknesses $D \simeq 5$ nm [1–3]. In either the CBF or NBF case, the measured thickness suggests that there is room for only a few layers of water molecules separating the two opposite monolayers, providing a natural nanoconfinement of the water.

Both static and dynamic responses as well as thermodynamic properties of nanoconfined water show significant quantitative or even qualitative differences from macroscopic predictions. S. Han et al. [4] have recently reported simulation results for TIP5P water in a quasi-two-dimensional hydrophobic nanopore slit. Studying phase transitions in the extremely strong confined water nanofilms as a function of the temperature, the authors found results consistent with the idea that water might freeze by means of both first-order and continuous phase transitions, depending on the density or pressure, while a first order transition line between solid and liquid phases is expected for bulk water. It is believed that the nature of the confining walls affects the freezing mechanism of water [5], as both in experiments [6] and in simulations [7] freezing has not been observed for water confined in hydrophilic environments. On the other hand, when water is confined by hydrophilic surfaces, it has a strong interaction with the walls and its dynamical properties can change dramatically [8–10]. For instance, it has been predicted that at low water content conditions and areas per surfactant close to experimental estimates in NBFs, homogeneous films undergo an adhesion transition [11,12]. Furthermore, it has been also recently demonstrated that nanoconfined water under electric field at constant chemical potential undergoes electrostriction [13].

The different underlying molecular mechanisms, which are often hard to approach by direct experiments or even analytically, can be explored by numerical simulations. For instance, surface interactions of nanoscaled black films in terms of the disjoining pressure and the wetting transition theory have been recently studied using the molecular simulation method [14,15,12].

When analyzing the stability of the films, one of the key quantities is the free energy of the system under study as well as its chemical potential. The free energy determines the equilibrium physics, and free energy differences determine chemical equilibrium and dynamics. From a thermodynamic point of view, transport processes are governed by the free energy gradient of moving molecules. Thus, the calculation of the free energy profiles across their path can shed some light on the

E-mail address: dinapoli@tandar.cnea.gov.ar.

https://doi.org/10.1016/j.chemphys.2018.07.033
Received 31 May 2018; Accepted 22 July 2018
Available online 01 August 2018
0301-0104/

physicochemical background of their transport. The calculation of solvation free energies is a computationally far more demanding task than the generation of an equilibrium ensemble by computer simulations. This difficulty is enhanced in inhomogeneous systems, such as lipid bilayers that combine aqueous, hydrophobic and hydrophilic regions. In spite of this, there exist several techniques for computing the chemical potential of a given species in a single Monte Carlo (MC) or Molecular Dynamics (MD) simulation and we will apply several of these techniques in this work, where we study the thermodynamic properties of bulk and nanoconfined water in a natural hydrophilic environment, as are the Newton black films. We address this problem with a simplified amphiphilic model that nevertheless takes into account the strong electrostatic interactions and intramolecular amphiphilic modes, by including a charged semiflexible chain model and the TIP5P model of water [16,17,8].

2. Molecular models and molecular dynamics simulations

The intermolecular potential of water molecules in our MD simulations is described by the classical and rigid molecular model TIP5P [18,19].It consists of one Lennard-Jones (LJ) site localized at the O atom and four charges. Two positive charges are localized at the H atoms and two negative charges at the lone pairs. This water model gives good results for the calculated energies, diffusion coefficients and density of water as a function of temperature, including the anomaly in the density near 4 °C and 1 atm [18].

Our amphiphilic model corresponds to a simplification of sodium dodecyl sulfate (SDS) $[CH_3(CH_2)_{11}OSO_3^-Na^+]$ in solution. Our negatively charged amphiphilic consists in a semiflexible chain of 14 atoms, in which the bond lengths are held constant but bending and torsional potentials are included, in order to simulate the molecular stiffness and to avoid an artificial molecular collapse. The first two atoms of the chain mimic a charged and polar head (atom 1 with a charge of $-2e$, atom 2 with a charge of 1e) and their Lennard Jones parameters are: $\sigma_1 = \sigma_2 = 4.0$ Å, $\epsilon_1 = 2.20$ kJ/mol, kJ/mol. The following 12 uncharged atoms form the hydrophobic tail: sites 3–13 are united atom sites CH_2 and site 14 is the united atom site CH_3. We are also including a Na^+ ion per chain in the MD box. Full details on the molecular geometry, charge distribution, inter- and intra-molecular potential parameters are given in [17,20] and references therein.

To obtain the equilibrated configurations for the chemical potential computation, we integrate the equations of motion of all molecules using the velocity Verlet algorithm for the atomic displacements and the SHAKE and RATTLE algorithms for the constant bond length constraints on each molecule. The electrostatic interactions are calculated by using the Ewald's sums for quasi-bidimensional samples with a cut-off radius of 12 Å [16,17]. The time step is 2 fs, the samples are thermalized typically for 20 to 200 ps, and measured over a free MD trajectory for the following 2 ns. Our MD simulations are performed with a code developed in our group and use the Berendsen algorithm to maintain the constant temperature of the samples [21].

We perform MD simulations on samples of 500 water molecules for the bulk water case and samples containing 256 amphiphilics plus 2 water molecules per amphiphilic in the case of confined water. The initial configuration of the pure water consists of 4-water molecules on a face centered square lattice of $5 \times 5 \times 5$ unit cells, with lattice constant $a = 4.943$Å, while the corresponding configuration for the NB-film is totally similar to that used in Refs. [8,9]. It consists of a pre-assembled bilayer, that is built by arranging half of the chain molecules on a body centered square lattice of 8x8 unit cells, in the (x, y) plane, with lattice constant a. The molecular center of mass of the modeled SDS anions are initially placed at $\left(\frac{1}{4}, 0, \pm z_c\right)$ and $\left(\frac{3}{4}, \frac{1}{2}, \pm z_c\right)$, with the headgroups pointing to the core of the bilayer, which results in an initial distance between tail to tail chain layers greater than twice the final measured distance of less than 45Å, in the equilibrated sample

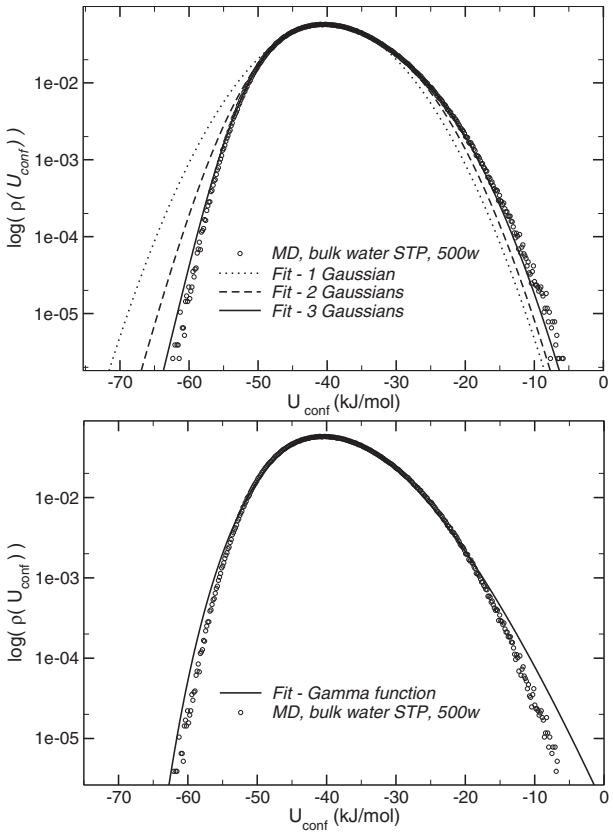

Fig. 1. Measured distribution $\rho(U)$ and its approximations by one to three Gaussian functions (top) and by the Gamma function introduced in Ref. [22]. (bottom).

(See in Fig. 4 an atomic density profile, $D(z)$, as a function of the bilayer normal distance z and a snapshot of the equilibrated sample).

3. Excess free energy and chemical potential of bulk water

3.1. Free energy and the quasi-Gaussian approximation

The quasi-Gaussian approximation for the determination of the Helmholtz free energy was introduced by A. Amadei et al. [22], based on the fact that at not too low temperature a macroscopic system can be regarded as an infinite collection of identical independent subsystems and, therefore, the potential energy distribution function should be close to a Gaussian. In the NVT (canonical) ensemble, the excess free energy F', relative to the averaged configuration energy $U_1 = \langle U_{conf} \rangle$, is given by:

$$F' = U_1 + kT \ln(\langle \exp(\beta(U - U_1)) \rangle), \tag{1}$$

where the average is calculated as:

$$\langle \exp(\beta(U - U_1)) \rangle = \int \exp(\beta(U - U_1)) \rho(U) dU.$$

In the upper panel of Fig. 1 we include the potential energy distribution function $\rho(U)$ obtained in our MD simulation of the sample of 500 water molecules at STP. Following Ref. [22], this distribution function $\rho(U)$ can be fitted, in a first approximation, by a Gaussian function $\left(\rho(U) = \frac{1}{\sigma\sqrt{2\pi}} exp\left(-\frac{(U-U_1)^2}{2\sigma^2}\right)\right)$ and, therefore the excess free energy is:

$$F' \cong U_1 + kT \ln\left(\exp\left(\frac{\beta^2\sigma^2}{2}\right)\right) = U_1 + \frac{\beta\sigma^2}{2} \tag{2}$$

In Ref. [22] it is also suggested, as a second approximation to $\rho(U)$, the uninormal Gamma function (their formula (69)). The Gamma

Table 1
Calculated values of F' obtained from our MD distribution $\rho(U)$ and several fits with up to three Gaussian functions and the Gamma function, shown in Fig. 1. Unit: kJ/mol

	$\langle U_1 \rangle$	F′
1 G	−40.1	−30.4
2 G	−39.3	−29.4
3 G	−38.9	−28.3
MD	−38.9	−27.9
Gamma		−24.5
Ref. [22]		−24.0

function is the first physically acceptable solution of $\rho(U)$ just beyond the Gaussian distribution, having three adjustable parameters, given by $\Gamma(\frac{b_0}{b_1^2}) = \int_0^\infty x^{b_0/(b1^2-1)}\exp(-x)dx$. Approximations of higher orders rapidly become cumbersome analytical functions. Due to the increasing analytical complexity of this approach and its lengthy convergence, we decided instead of using the suggested functions, to fit our measured distribution $\rho(U)$ by a sum of Gaussian functions. We include up to three Gaussian functions in the fit and our calculated functions are also shown in the upper panel of Fig. 1.

When dealing with a sum of Gaussian functions, it is important to note that since the energy distribution function $\rho(U)$ is that of a macroscopic system, it must be uninormal, that is:

$$\rho(U) = \sum_i \frac{a_i}{\sigma_i\sqrt{2\pi}} exp\left(-\frac{(U-U_i)^2}{2\sigma_i^2}\right),$$

with $\sum_i a_i = 1$. In this case, the excess free energy is given by:

$$\exp(\beta F') = \sum_i a_i \exp(\beta U_i + \beta^2\sigma_i^2/2). \tag{3}$$

In Table 1 we show the excess free energy values calculated with several approximations to $\rho(U)$. From the data of this Table and Fig. 1, we can conclude that this method gives a lower limit of F' (a more negative value) because the Gaussians give a lower limit to the measured MD distribution.

If the Gamma function is used as a second approximation to $\rho(U)$ (Eq. (63) of Ref. [22]) we obtain the data shown in the lower panel of Fig. 1 and Table 1. The Gamma function clearly gives an upper limit to F'. In Fig. 1 of Ref.[22], the excess free energy F' of liquid water as a function of temperature is shown, for several approximations as well as for the experimental case. It can be seen from that figure that $F'(T = 300\ \text{K}) \simeq 24.0$ kJ/mol, in good agreement with our obtained value.

3.2. Chemical potential, the insertion and deletion methods and the overlapping distribution method

The chemical potential μ is defined such that the Helmholtz free energy F changes by μdN, when the number of particles changes by dN, at constant T and V. For computing the chemical potential of not too dense atomic or simple molecular liquids, one of the most used methods is the Widom's insertion one [23]. Within this method, a 'ghost' particle insertion is considered at a random point in an arbitrary simulation step, the interaction energy between the 'ghost' and all molecules in the host is computed and the 'ghost' is removed. The excess chemical potential, with respect to an ideal gas phase, can be calculated as:

$$\mu_{ex}^{ins} = \Delta F = -kT\ln\langle\exp(-\beta U_g)\rangle_N$$
$$= -kT\ln\int \rho_{ins}(U)\exp(-\beta U_g)dU \tag{4}$$

where U_g is the potential energy interaction of an inserted 'ghost' water molecule with the system containing N molecules. Fig. 2 includes the energy distribution $\rho_{ins}(U)$ of an inserted 'ghost' molecule in the bulk sample of water, obtained after 3×10^6 random insertion trials. Further

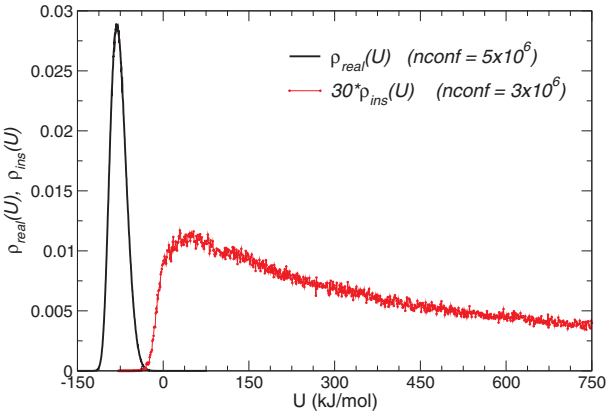

Fig. 2. Bulk water, 500 w, measured distributions of the interaction energy of one molecule with its neighbors $\rho_{real}(U)$ and that of an inserted ghost molecule with the whole system $\rho_{ins}(U)$.

increase in the number of trials does not change the maximum location and its value, but improves the distribution in the range of low energies. The main contribution to the integrand in Eq. 4 is in the range of low energies (essentially the negative values). From a total of 3×10^6 insertion trials, only 12389 define $\rho_{ins}(U)$ at negative energies, and therefore the numerical calculation gives a rough estimation of −18.5 kJ/mol.

The Widom insertion technique is limited to small particles and to systems at low or moderate densities. To obtain a reliable estimate of the insertion probability, $\langle\exp(-\beta U_g)\rangle_N$, and thus an accurate value for the chemical potential, it is necessary to reach regions of the configurational space where U_g is low. For systems at high densities, as in our case, the majority of random insertions results in an overlap with the repulsive core of a particle in the system, and contributes negligibly to the insertion probability. Under these circumstances, a huge number of simulations would be required in order to obtain μ_{ex} with good statistical accuracy.

Alternatively, the chemical potential can also be calculated by "freezing" the simulated fluid and temporarily removing a particle from the system. In the so-called "real" or "inverse" Widom method of Shing and Gubbins [24] the excess chemical potential of a pure fluid is given by

$$\mu_{ex}^{real} = kT\ln\langle\exp(\beta U_r)\rangle_N$$
$$= kT\ln\int \rho_{real}(U)\exp(\beta U)dU \tag{5}$$

where U_r is the interaction energy of a real molecule with all other molecules. While in the "ghost particle" method the ghost is not a member of the ensemble of $N + 1$ particles, in the "real particle" method the interaction energy U_r is that of a molecule belonging to the ensemble. In Fig. 2 we show the energy distribution $\rho_{real}(U)$ obtained in our MD sample of 500 water molecules.

As already mentioned, the main disadvantage of the ghost-particle method is that at high densities only a few random insertions happen to be into a "hole" in the system. Most random insertions of a ghost result in overlaps, therefore sampling low-energy configurations inefficiently. On the other hand, the real particle method suffers from the opposite problem, that is, as the real particle is already in the fluid, high energies are not sampled efficiently. A more accurate method [24] to calculate the excess chemical potential is given by the *overlapping distribution method* (OD), which combines the insertion and deletion methods. It was introduced by Shing and Gubbins [24] through the relationship:

$$\rho_{ins}(U)exp(-\beta U) = \rho_{real}(U)exp(-\beta\mu_{ex}). \tag{6}$$

where $\rho_{ins}(U)$ and $\rho_{real}(U)$ are the distributions depicted in Fig. 2.

The relationship (6) means that at the energy U_{cross}, where both normalized distributions intercept, we get $U_{cross} = \mu_{ex}$. To obtain the

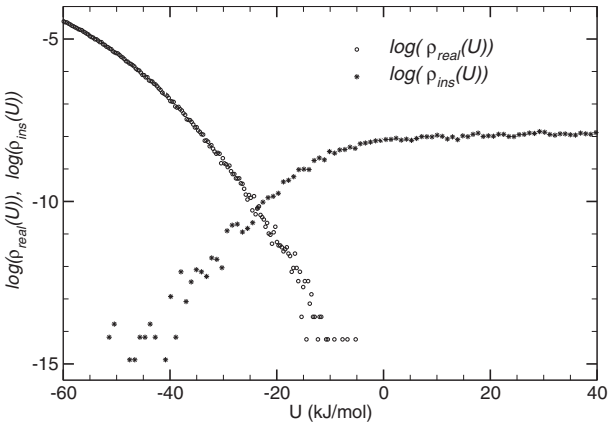

Fig. 3. Logarithmic graph of the distributions in Fig. 2, in the range of energies where they superpose.

value of μ_{ex} we use a logarithmic plot in the range of energies where both distributions superpose (Fig. 3). The following relationship is used and the value of μ_{ex} is obtained through a linear fit:

$$log(\rho_{real}(U)) - log(\rho_{ins}(U)) + \beta U = \beta\mu_{ex} \quad (7)$$

From Fig. 3, the logarithm of both distributions intercept at $U \simeq$-24.0(5) kJ/mol. From Ref. [25], the experimental chemical potential of water at STP is $\mu^{exp} = \mu_{ideal} + \mu_{ex} = -54.80$ kJ/mol. In Ref. [26] the obtained chemical potential of bulk rigid CHARMM-TIP3P water molecules at 298 K and 0.1 MPa is -55.29 kJ/mol calculated with the OD method [24,27] and -50.20 kJ/mol calculated within the Cavity Insertion Widom (CIW) method [28]. It is important to note that all these values are for the chemical potential μ and not for the excess chemical potential we are calculating, $\mu_{ex} = \mu - \mu_{ideal}$, where μ_{ideal} is the ideal gas chemical potential at the same average density as the pure water system. Within our NVT conditions, the ideal value $\mu_{ideal} = -30.09$ kJ/mol, calculated as if the water molecules were an ideal gas at the present density. In Ref. [29] the excess chemical potential of bulk water, obtained from a MD simulation of 256 molecules at 300 K, density $\rho = 0.987$ gr/cm^3 and using the TIP3P model, is $\mu_{ex}^{w} = -25.307$ kJ/mol. In Table 2 we summarize the mentioned values and we show our obtained results. It can be seen from Tables 1 and 2 that the third order in the quasi-Gaussian approximation as well as the Gamma function and our last method give the best calculated values for the excess free energy and the excess chemical potential, respectively.

4. Excess free energy and chemical potential of nanoconfined water in a NB-film

4.1. Free energy and the quasi-Gaussian approximation

As stated in Section 2, our NB film is modeled by 256 amphiphilic molecules plus 2 water molecules per amphiphilic. In Fig. 4 (top) we show the atomic density profile, $D(z)$, as a function of the bilayer normal distance z and a snapshot of the equilibrated sample (bottom).

Table 2
Chemical potential (μ) of bulk water. Note that $\mu_{ex} = \mu - \mu_{ideal}$, where $\mu_{ideal} = -30.09$ kJ/mol calculated as if the water molecules were an ideal gas at the present density. (OD) Calculated using the overlapping distribution method, (CIW) by means of the Cavity Insertion Widom method and (TI) through a thermodynamic integration.

Reference and method	μ (kJ/mol)	μ_{ex} (kJ/mol)
This work, TIP5P (OD)	−54.09	−24.00
[25], exp	−54.80	
[26], CHARMM-TIP3P (OD)	−55.29	
[26], CHARMM-TIP3P (CIW)	−50.20	
[29], TIP3P		−25.307
[30], TI	54.06	

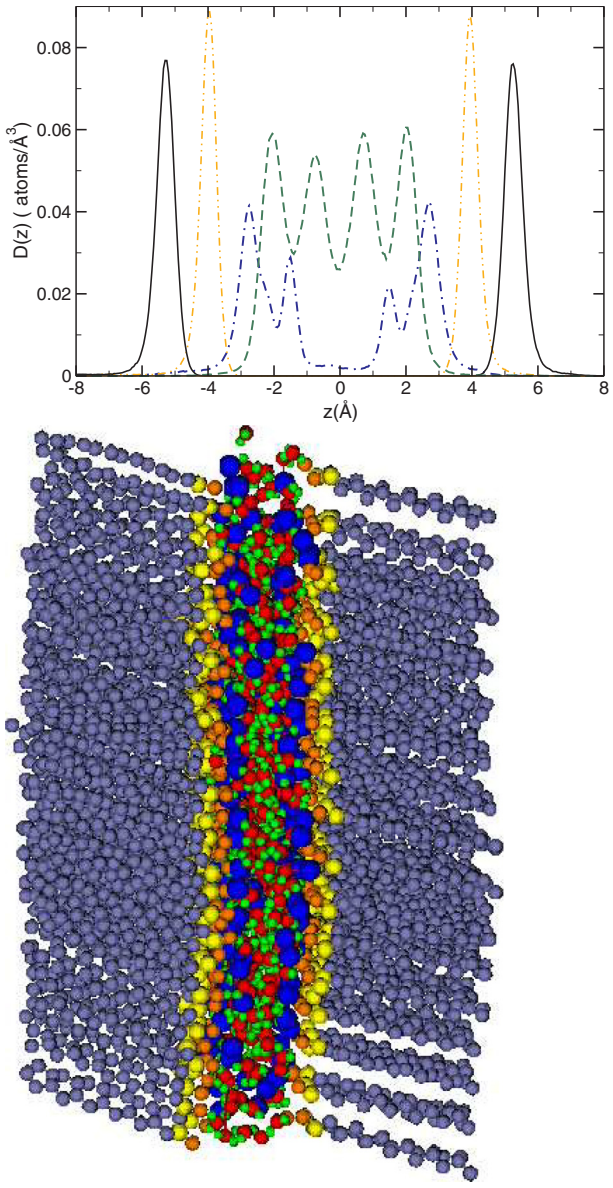

Fig. 4. (top) Atomic density profile, $D(z)$ (i.e.:number of atoms per Å^3) of our NB film consisting of 256 amphiphilics, 256 Na^+ ions plus 2 water molecules per amphiphilic. $z = 0$ at the core of the bilayer. Continuous black: atom 1 of polar head, dot-dot-dashed orange: atom 2 of polar head, dot-dashed blue: Na^+ ions and dashed green: O of water molecules. (bottom) Snapshot of the equilibrated bilayer described in the top panel. Grey: amphiphilic tails, orange-yellow: amphiphilic heads, blue: Na^+ ions and red-green: water molecules. (For interpretation of the references to colour in this figure legend, the reader is referred to the web version of this article.)

The potential distribution function for water molecules in our bilayer is shown in Fig. 5. It can be integrated numerically, obtaining an average potential energy of -59.2 kJ/mol and a free energy of -37.9 kJ/mol. This distribution function can be fitted with two Gaussian functions, one we assume is for the water in contact with head groups and other for water deep inside the bilayer. From the fit we obtain the following values: 68% of the water molecules correspond to a distribution with an averaged potential energy of -53.8 kJ/mol, with a deviation of 8.2 kJ/mol, and the other 32% have an averaged potential energy of -70.5 kJ/mol, with a deviation of 7.7 kJ/mol. The

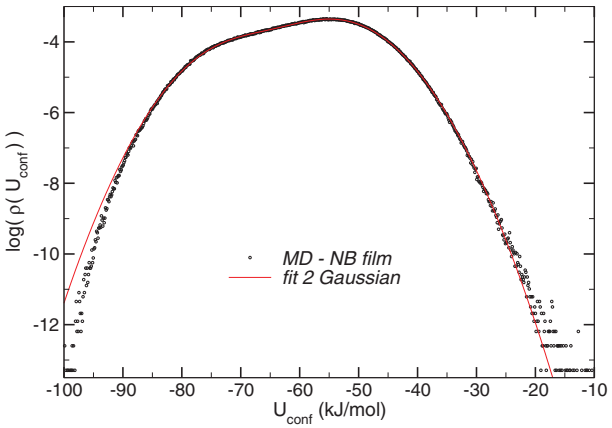

Fig. 5. Logarithmic measured configurational energy distribution (U_{conf}) and the corresponding fit with two Gaussian functions, for the confined water in the NB film.

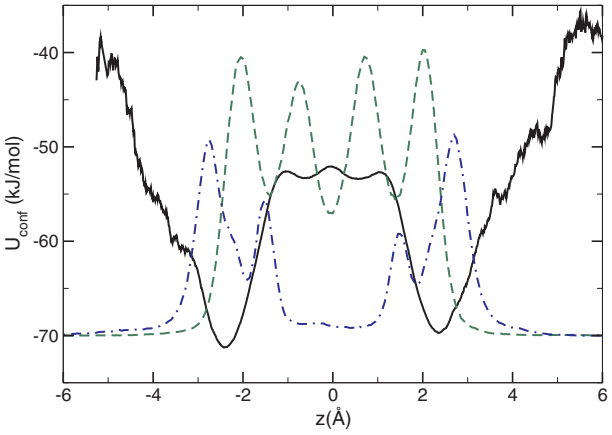

Fig. 6. Configurational energy profile of water confined in the NB film as a function of the bilayer normal distance z (continuous black line). Density profiles of Na^+ (dot-dashed blue) and O of water molecues (dashed green) are included (out of scale) for clarity.

fraction more tightly bound are those in the neighborhood of amphiphilic heads, as is determined by the profile of Fig. 6. The calculated free energy of the first group of molecules is -40.3 kJ/mol and that of the second is -58.4 kJ/mol. That is, there is a difference of -16.7 kJ/mol in the potential energy and of -18.1 kJ/mol in the free energy between the second and first group of molecules. In other words, the free energy of water molecules located at the center of the film is greater than the corresponding free energy of water molecules lying closer to the amphiphilic heads, but still is lower than the free energy of bulk water due to the strong interaction with the polar heads.

4.2. Chemical potential and the overlapping distribution method

As concluded in the previous section, the OD method gives our best calculated value of the chemical potential in the case of bulk water. Therefore, we combine the insertion and deletion energy distribution of a water molecule in the core of the NB film. Fig. 7 (top) includes the energy distribution of deleting one water molecule, and Fig. 7 (middle) is the energy distribution of an inserted 'ghost' water molecule within the core of the bilayer. Although the energy distributions $\rho_{real}(U)$ and $\rho_{ins}(U)$ do not intercept, from the analytical continuity distribution of ρ_{real} we can get a rough estimate of $\mu_{ex} \simeq -24.8 \pm 0.6$ kJ/mol. In the bottom panel of Fig. 7 we show the logarithmic plots and the intersection of the above mentioned distributions.

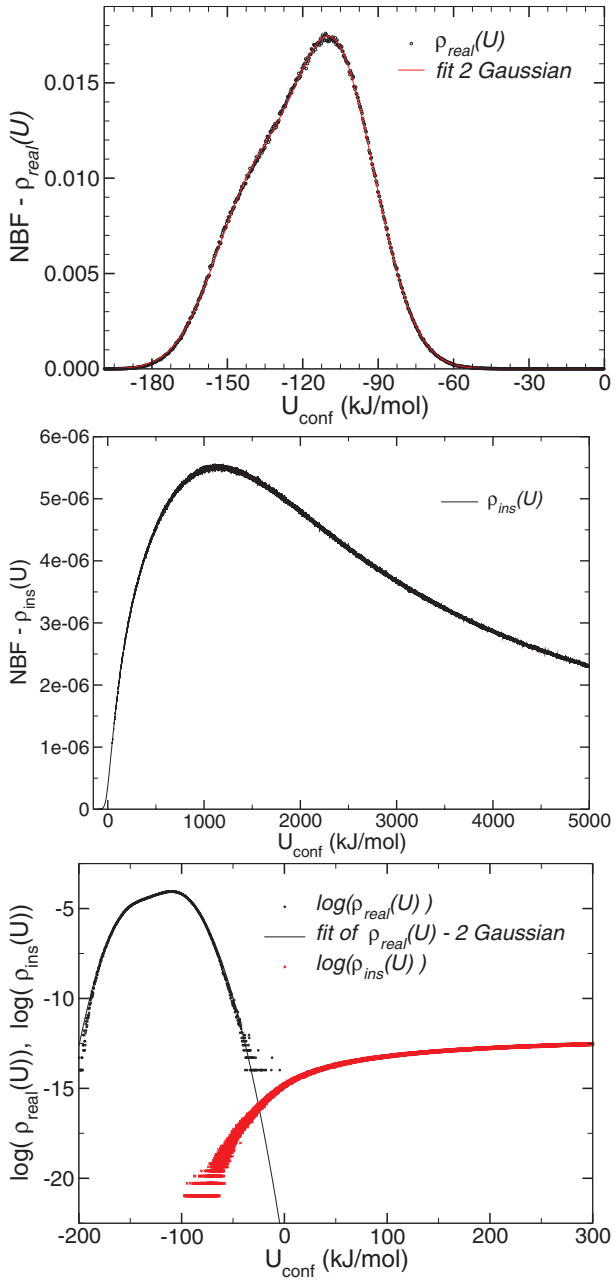

Fig. 7. (top) Distribution of energies of a real water molecule in the core of the NB film, calculated from 5.12×10^6 trial configurations; (middle) distribution of energies for an inserted ghost water molecule also within the core of the bilayer, after 3×10^{10} trial configurations; (bottom) logarithmic plots of the distributions $\rho_{real}(U)$ and $\rho_{ins}(U)$.

Even when the OD method is more precise than the other explored methods when it is used for calculating the chemical potential of bulk water, it gives just a rough idea of the chemical potential in the case of nanoconfined water. This is because we cannot separate the contributions from the molecules located at the center of the film from the ones lying closer to the amphiphilic heads. To this end we introduce, in the next subsection, free energy profiles along the axis normal to the bilayer z.

4.3. Free energy profile: the probability ratio method

A method to measure the free energy barrier, also tested in a biological membrane in Ref. [26], is the density probability ratio. This

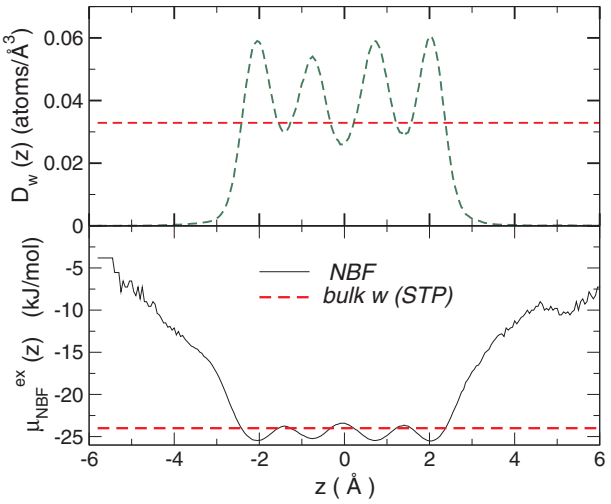

Fig. 8. (top) Density profile of water molecules $D_W(z)$ in the bilayer and (bottom) chemical potential or free energy profile of the TIP5P water molecule along the bilayer normal (z), calculated using Eq. (9). We show the corresponding values of bulk water in both figures, for comparison.

method calculates the free energy difference along the z axis using:

$$\Delta F(z) = F(z) - F(z_0) = -kT \ln\left(\frac{D_w(z)}{D_w(z_0)}\right) \tag{8}$$

where z_0 is usually taken at the center of the bilayer, that is $z_0 = 0$ and $D_w(z)$ is the profile of the density distribution function of water across the bilayer (See Fig. 4). This method gives good results for differences in the free energy in the region where the density of water is well determined [26]. Its main problem is that, with this formulation, and due to the decreasing (to zero) density of water, the difference of energy between a molecule of water inside and outside the core of the NB film, cannot be determined. If, instead, we take bulk water as the reference system, we can obtain the absolute free energy of water in the NB film core. Using the same density profile of water, and following the method of Ref. [29], we can calculate the difference between the excess chemical potential of water in the core of the bilayer and that of bulk water:

$$\frac{D_w(z)}{D_{wbulk}} = \exp(-\beta(\mu^{ex}_{NBF}(z) - \mu^{ex}_{bulk})). \tag{9}$$

Assuming that the data on bulk water are well known, we can obtain absolute values of $\mu^{exc}_{wNBF}(z)$. According to Fig. 8, in the core of the bilayer is $-25.52\,\text{kJ/mol} < \mu^{ex}_{NBF}(z) < -23.41\,\text{kJ/mol}$, with our calculated value of $\mu^{ex}_{bulk} = -24.0(5)$ kJ/mol and $D_{wbulk} = 0.0329$ water molecules per Å^3, at STP. Therefore we find that, depending on the position of the water molecule, the chemical potential is slightly lower than the corresponding to bulk water, suggesting that a water molecule might be more stable within the slab than in bulk water, as also obtained for a water molecule in a lipid membrane [26]. Similar values of chemical potential for water under nanoconfinement in other systems were obtained. For example, for water confined in a nanotube of 8.1Å the excess chemical potential was found to be ~ -28.744 kJ/mol [29], also showing more stability than in bulk water. Also seen from Fig. 8, the stability of the water molecules decreases when moving towards the hydrophobic tails.

5. Summary and discussion

In this work we explore several approximations to the calculation of the free energy and excess chemical potential of water molecules within two different environments, namely bulk water and under a natural nanoconfinement provided by a NB film. We use a charged semiflexible amphiphilic model and the TIP5P model of water in our molecular dynamic simulations.

In the case of bulk water, we find that both the third order in the quasi-Gaussian approximation and the Gamma function lead to results that compare well with previously reported values. Nevertheless, it is the OD method that exhibits an excellent agreement with the experimentally obtained value of the chemical potential for bulk water.

When considering the water molecules under confinement we find, already by means of the quasi-Gaussian approximation, that the free energy of water molecules which are assumed to be located at the center of the film, is greater than the corresponding free energy of water molecules lying closer to the amphiphilic heads, but which is still lower than the free energy of bulk water, due to the strong interaction with the polar heads.

To completely characterize our system, we calculate the free energy profile of the water molecules along the bilayer normal. Our results suggest that a water molecule is more stable in some regions of the Newton black film than in bulk water. This trend of stability is also supported by the results obtained from the OD method, as the calculated value by means of this last method is also slightly lower than that of bulk water.

Acknowledgment

Dr. S. Di Napoli is grateful to Dr. Zulema Gamba for initializing her in this topic.

References

[1] G. Gochev, D. Platikanov, R. Miller, Adv. Colloid Interface Sci. 233 (2016) 115.
[2] A. Reinold, A. Ruecker, Phil. Trans. Roy. Soc. London A 184 (1893) 505.
[3] E. Johonnott, Phil. Mag. 47 (1899) 501.
[4] S. Han, M.Y. Chai, P. Kumar, H.E. Stanley, Nature Phys. 6 (2010) 685.
[5] J. Mittal, G. Hummer, Faraday Discuss. 146 (2010) 341.
[6] U. Raviv, P. Laurat, P. Klein, Nature 413 (2001) 51.
[7] K. Koga, H. Tanaka, X. Zeng, Nature 408 (2000) 564.
[8] S.D. Napoli, Z. Gamba, J. Chem. Phys. 132 (2010) 075101.
[9] S.D. Napoli, Z. Gamba, Phys. B 404 (2009) 2883.
[10] M. Chen, X. Lu, X. Liu, Q. Hou, Y. Zhu, H. Zhou, Phys. Chem. Chem. Phys. 17 (2015) 19183.
[11] F. Bresme, E. Chacón, H. Martínez, P. Tarazona, J. Chem. Phys. 134 (2011) 214701.
[12] P. Tarazona, H. Martínez, E. Chacón, F. Bresme, Phys. Rev. B 85 (2012) 085402.
[13] D. Vanzo, D. Bratko, A. Luzar, J. Chem. Phys. 140 (2014) 074710.
[14] T. Peng, M. Firouzi, Q. Li, K. Peng, Phys. Chem. Chem. Phys. 17 (2015) 20502.
[15] T. Peng, Q. Li, L. Xu, C. He, L. Luo, Entropy 19 (2017) 620.
[16] I.-C. Yeh, M.L. Berkowitz, J. Chem. Phys. 111 (1999) 3155.
[17] Z. Gamba, J. Chem. Phys. 129 (2008) 164901.
[18] M.W. Mahoney, W.L. Jorgensen, J. Chem. Phys. 112 (2001) 8910.
[19] M.W. Mahoney, W.L. Jorgensen, J. Chem. Phys. 114 (2001) 363.
[20] Z. Gamba, J. Chem. Phys. 129 (2008) 215104.
[21] H. Berendsen, J. Postma, W. van Gunsteren, A. DiNola, J. Haak, J. Chem. Phys. 81 (1984) 3684.
[22] A. Amadei, M.E.F. Apol, A.D. Nola, H.J.C. Berendsen, J. Chem. Phys. 104 (1996) 1560.
[23] B. Widom, J. Chem. Phys. 39 (1963) 2802.
[24] K.S. Shing, K.E. Gubbins, Mol. Phys. 46 (1982) 1109.
[25] A. Ben-Naim, Y. Marcus, J. Chem. Phys. 81 (1984) 2016.
[26] K. Shinoda, W. Shinoda, M. Mikami, J. Comput. Chem. 29 (2008) 1912.
[27] C. Bennet, J. Comp. Phys. 22 (1976) 245.
[28] P. Jedlovszky, M. Mezei, J. Am. Chem. Soc. 122 (2000) 5125.
[29] G. Hummer, J.C. Rasalah, J.P. Noworyta, Nature 414 (2001) 188.
[30] M. Shirts, V. Pande, J. Chem. Phys. 119 (2003) 5740.